MICHIGAN STATE
UNIVERSITY

National Superconducting Cyclotron Laboratory

ROLE OF INTRUDER CONFIGURATIONS IN ^{26,28}Ne AND ^{30,32}Mg

B.V. PRITYCHENKO, T. GLASMACHER, P.D. COTTLE, M. FAUERBACH, R.W. IBBOTSON, K.W. KEMPER, V. MADDALENA, A. NAVIN, R. RONNINGEN, A. SAKHARUK, H. SCHEIT, and V.G. ZELEVINSKY

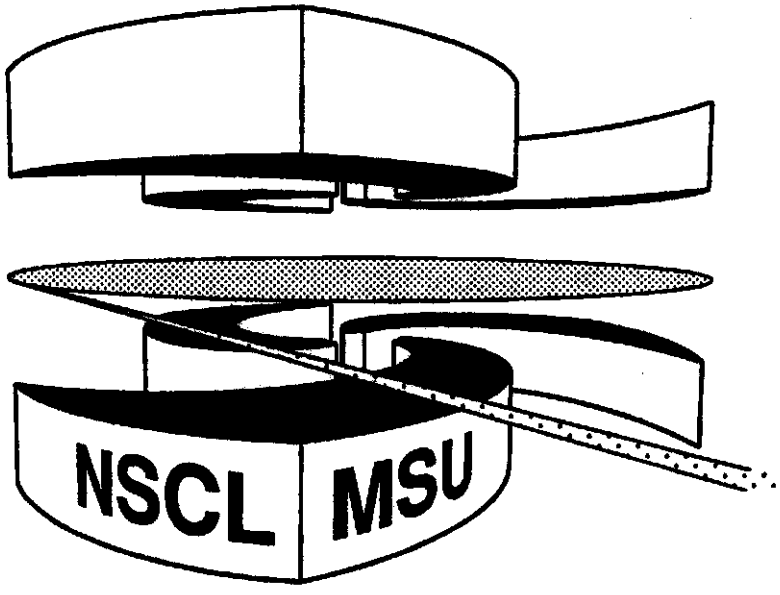

MSUCL-1128 **JULY 1999**

MSUCL-1128, submitted to Physics Lett. B

Role of intruder configurations in ^{26,28}Ne and ^{30,32}Mg

B. V. Pritychenko[1,2], T. Glasmacher[1,2], P.D. Cottle[3], M. Fauerbach[3], R.W. Ibbotson[1*], K.W. Kemper[3], V. Maddalena[1,2], A. Navin[1†], R. Ronningen[1], A. Sakharuk[1], H. Scheit[1,2‡] and V. G. Zelevinsky[1,2]

[1] *National Superconducting Cyclotron Laboratory, Michigan State University, East Lansing,* Michigan *48824*

[2] *Department of Physics* and *Astronomy, Michigan State University, East Lansing,* Michigan *48824*

[3] *Department of Physics, Florida State* University, Tallahassee, Florida *32306*

(July 12, 1999)

Abstract

The energies and reduced transition probabilities $B(E2; 0^+_{g.s.} \rightarrow 2^+)$ for the lowest $J^\pi = 2^+$ excited states in the neutron-rich radioactive isotopes ^{26,28}Ne and ^{30,32}Mg were measured via intermediate energy Coulomb excitation. The data suggest that the interaction between coexisting $0\hbar\omega$ (normal) and $2\hbar\omega$ (intruder) configurations signficantly perturbs the energy of the 2^+_1 state in ^{28}Ne, while the data on ^{26}Ne and ^{30}Mg can be well understood in the context

*Present address: Cyclotron Institute, Texas A&M University, College Station, Texas 77843-3366

†Permanent address: Nuclear Physics Division, Bhabha Atomic Research Centre, Bombay 400085, India

*Present address: Max-Planck-lnstitut für Kemphysik, Postfach 10 39 80, D-69029 Heidelberg, Germany

of $0\hbar\omega$ configurations alone. Nilsson model calculations suggest that if these nuclei have static axially symmetric deformations, they are prolate.

27.30.+t,25.70.De,23.20.Js

Measurements of nuclear masses, level energies and electromagnetic matrix elements in a group of neutron-rich nuclei in the vicinity of ^{32}Mg have indicated the existence of an "island of inversion" in which isotopes at or near the $N = 20$ shell closure have large deformations. The observation of binding energies considerably larger than those expected from conventional shell model calculations provided the first evidence for large deformations in this region [1–5]. Further support for the existence of the island of inversion was supplied by the measurement of an anomalously low energy for the 2_1^+ state in the $N = 20$ isotope ^{32}Mg [6] and a large value for the reduced matrix element $B(E2; 0_{gs}^+ \rightarrow 2_1^+)$, which indicated a quadrupole deformation parameter of $\beta_2 \approx 0.5$ [7].

It was found after the observation of overbinding that large deformations in this region could be explained by invoking excitations of pairs of neutrons across the $N = 20$ shell gap ($2\hbar\omega$ configurations). In a small set of nuclei - the island of inversion - these coexisting $2\hbar\omega$ "intruder" states actually fall below the "normal" $0\hbar\omega$ states to become the ground state configurations. The first calculations of this kind were performed in the Hartree-Fock framework [8], but it soon became clear that the island of inversion was an important challenge for the shell model [2,9]. Shell model calculations of increasing complexity [5,10–14] and calculations in other frameworks [15–18] have been performed, but important gaps have remained in the spectroscopic data.

In this letter, we report on an experimental study of the spectroscopy of the low-lying states in ^{26,28}Ne and ^{30,32,34}Mg - which are located both in the island of inversion and on its periphery - using the technique of intermediate energy Coulomb excitation with radioactive beams. These results include the first measurements of $B(E2; 0_{gs}^+ \rightarrow 2_1^+)$ in ^{26,28}Ne and ^{30}Mg. Our results provide a more complete picture of the extent of the island of inversion and the role of the intruder states outside the boundaries of the island of inversion. We find that the energies and $B(E2; 0_{gs}^+ \rightarrow 2^+)$ values for the lowest 2^+ states in the $N = 16$ isotope ^{26}Ne and the $N = 18$ isotope ^{30}Mg can be explained using the normal $0\hbar\omega$ configurations, while the energy of the 2_1^+ state in ^{28}Ne suggests strong mixing between the intruder and normal configurations in this nucleus. We also present deformed shell model calculations which

suggest that if these nuclei have static axially symmetric deformations, they are prolate.

The technique of intermediate energy Coulomb excitation of radioactive beams has now been used to measure energies of excited states and electromagnetic matrix elements in variety of nuclei, particularly of masses less than 60 (for a review, see [19]). In general, the projectile nucleus scattering off a target nucleus may be excited through nuclear or Coulomb interactions. At laboratory frame projectile energies of approximately 50 MeV/nucleon, Coulomb excitation dominates the inelastic scattering process at scattering angles of less than θ_{lab}=4.0°. Therefore we limit our experiment to such small scattering angles and can neglect the nuclear contribution.

The present experiments were performed at the National Superconducting Cyclotron Laboratory (NSCL) at Michigan State University, and the primary beams for the present experiment were produced with the NSCL superconducting electron resonance ion source and the K1200 superconducting cyclotron. A primary beam of $^{48}Ca^{13+}$ with an energy up to 80 MeV/nucleon and intensity as high as 8 particle-nA was used to produce secondary beams of ^{28}Ne, ^{32}Mg and ^{34}Mg. The secondary beams of ^{26}Ne and ^{30}Mg were made with a primary beam of $^{40}Ar^{12+}$ having energies up to 90 MeV/nucleon and intensities as high as 80 particle-nA. The secondary beams were obtained via fragmentation of the primary beams in a thick ^{9}Be primary target (376 mg/cm^2 for the measurements with the ^{48}Ca primary beam, 564 mg/cm^2 for experiments with the ^{40}Ar primary beam) located at the mid-acceptance target position of the A1200 fragment separator [20].

Gold foils of thicknesses 518 mg/cm^2 (for the ^{26}Ne and ^{30}Mg measurements) and 702 mg/cm^2 (for the ^{28}Ne, ^{32}Mg and ^{34}Mg measurements) were used as secondary targets. After passing through the secondary target, the secondary beams were stopped in a cylindrical fast-slow plastic phoswich detector (called the "zero-degree detector", or ZDD) which allowed charge identification of the secondary beam particles. The ZDD detected secondary beam particles scattered into laboratory angles less than θ_{lab}=3.96° (for ^{26}Ne and ^{30}Mg) or less than θ_{lab}=2.80° (for ^{28}Ne and ^{32,34}Mg). The NSCL NaI(Tl) array [21] was used to detect photons in coincidence with the secondary beam particles. The secondary beams were run

in "cocktails" which contained several secondary beam species, while the ZDD and time of flight measurements in the beam line provided positive isotope identification. Typical beam rates for the particles of interest varied from a few to a few hundred per second.

The γ-ray spectra, both without the Doppler correction (so that the spectrum is seen in the laboratory frame) and with the Doppler correction (as seen in the projectile frame) for ^{26,28}Ne and ^{30,32,34}Mg are shown in Fig. 1. The laboratory frame and projectile frame spectra from a test measurement of the stable nucleus ^{36}Ar are also included to illustrate the Doppler shift technique. Photons deexciting the previously observed 2_1^+ states in ^{30}Mg and ^{32}Mg (at 1482 and 885 keV, respectively) are apparent in the projectile-frame spectra for those two nuclei. A strong peak occurs in the projectile-frame spectrum for ^{26}Ne at 1990(12) keV, while a somewhat weaker (though still clear) peak appears in the corresponding ^{28}Ne spectrum at 1320(20) keV. On the basis of these observations, we propose that the 2_1^+ states occur at these energies in ^{26,28}Ne. The results on the 2_1^+ state energies in the neon isotopes are consistent with those reported at a recent conference [22]. Only a few counts appear in the ^{34}Mg spectrum above a Doppler-shifted energy of 800 keV. Below this energy, there is background due to the Coulomb excitation of the gold target.

One other important feature in the ^{32}Mg spectrum is a small second peak in the spectrum at 1438(12) keV, an energy which agrees with a γ-ray observed at 1436(1) keV in the β-decay of ^{32}Na [23,24]. Klotz *et al.* [24] determined that the 1436 keV γ-ray is in coincidence with the 885 keV $2_1^+ \rightarrow 0_{gs}^+$ γ-ray and, therefore, that it deexcites a state at 2321 keV.

For ^{26,28}Ne and ^{30}Mg, where the 2_1^+ states do not appear to be fed by higher-lying states, the cross sections for populating the 2_1^+ states can be determined in a straightforward way, and they are listed in Table I. The population cross sections for the 2_1^+ states of these nuclei can then be used to obtain $B(E2; 0_{gs}^+ \rightarrow 2_1^+)$ values using the formalism of Winther and Alder [25], and these reduced matrix elements are also listed in Table I. The reliability of the present measurements is supported by the results of the test experiment using a secondary beam of the stable isotope ^{36}Ar, for which $B(E2; 0_{gs}^+ \rightarrow 2_1^+)$ is well established.

The analysis of the present data on ^{36}Ar yields $B(E2;0^+_{gs} \rightarrow 2^+_1) = 286(23)\ e^2fm^4$, which is in excellent agreement with the adopted value [26] of 298(30) e^2fm^4.

In the case of ^{32}Mg, the 2^+_1 state is not only populated directly in the intermediate energy Coulomb excitation reaction but is also fed via the 1436 keV γ-ray decay from the 2321 keV state. Therefore, the population cross section for the 2^+_1 state is the difference between the production cross sections for the 885 and 1436 keV γ-rays. Since the 885 keV transition has a well established $E2$ ($2^+_1 \rightarrow 0^+_{gs}$) character, the production cross section for this γ-ray can be unambiguously determined from the experimental yield to be 107(13) mb. However, there is some uncertainty about the cross section for production of the 1436 keV γ-ray because the efficiency for detection of a γ-ray depends on its angular distribution, which in turn depends on the multipolarity of the transition and the spins of the initial and final states. We do not know the spin and parity of the 2321 keV state; however, we can limit the possible J^π values for this state by requiring that the matrix elements $B(\lambda;0^+_{gs} \rightarrow \lambda^\pi)$ deduced from the experimental cross section corresponding to the observed yield for the 2321 keV state are less than or equal to the recommended upper limits listed by Endt [27]. This condition gives the possible J^π values for the 2321 keV state as 1^- (for which the measured cross section would give $B(E1;0^+_{gs} \rightarrow 1^-) = 0.040(16)\ e^2fm^2$), 1^+ (which gives $B(M1;0^+_{gs} \rightarrow 1^+) = 0.50(20)\ \mu_N^2$) or 2^+ (which gives $B(E2;0^+_{gs} \rightarrow 2^+) = 105(42)\ e^2fm^4$). The data on the β-decay of ^{32}Na do not provide any further constraints on the J^π values for this state. With the uncertainty for the J^π value for this state, we determine the cross section for production of the 1436 keV γ-ray to be 26(10) mb. When this is subtracted from the γ-ray production cross section for the 885 keV γ-ray, we obtain a cross section of 80(17) mb for direct population of the 2^+_1 state, which then yields $B(E2;0^+_{gs} \rightarrow 2^+_1) = 333(70)$ e^2fm^4 for ^{32}Mg. This result is consistent with that of Motobayashi *et al.* [7], 454(78) e^2fm^4. Without the feeding correction, we would obtain $B(E2;0^+_{gs} \rightarrow 2^+_1) = 440(55)\ e^2fm^4$.

The γ-ray deexciting the 2321 keV state directly to the ground state was not observed in the present experiment. The observation of this transition, which would provide important insights about the nature of the 2321 keV state, will be more likely with the more intense

beams and more sensitive detection instrumentation which will be available in the near future at next-generation facilities.

The secondary ^{34}Mg beam was particularly weak, and the integrated number of beam particles was small. However, we can still draw some conclusions from the γ-ray spectrum. The Doppler shifted spectrum for ^{34}Mg contains a significant background below 800 keV which results in part from γ-rays from the gold target. There are also several counts in the spectrum above 800 keV. The data are not sufficient to identify the energy of the 2_1^+ state. However, if we assume the 2_1^+ state is located between 0.9 and 1.4 MeV, we can place an upper limit on $B(E2; 0_{gs}^+ \rightarrow 2_1^+)$ of 670 e^2fm^4.

The island of inversion was originally identified by comparing experimental binding energies with predictions from a standard $0\hbar\omega$ model, as is shown in Fig. 2a where the experimental binding energy values [28] are compared with the $0\hbar\omega$ binding energies calculated by Warburton, Becker and Brown [5]. The experimental values are clearly at or close to the calculated $0\hbar\omega$ values at $N = 18$ and 19. The deviations become large at $N = 20$ and remain that way at $N = 21$. The experimental binding energy for ^{34}Mg ($N = 22$) also deviates strongly from the $0\hbar\omega$ value, while the data on ^{33}Na and ^{35}Mg are not precise enough to provide a conclusion for those isotopes. The masses indicate that the island of inversion includes the $N = 20$ isotopes of Ne, Na and Mg, the $N = 21$ isotopes of Na and Mg, and the $N = 22$ isotope of Mg. However, the binding energy data necessary to draw the upper mass boundary of the island of inversion are not available.

The data on 2_1^+ states reported here provide additional insights regarding the mechanisms at work around the island of inversion. The experimental values of the energies of the 2_1^+ states and $B(E2; 0_{gs}^+ \rightarrow 2_1^+)$ for the $N \geq 14$ Ne and Mg isotopes (data are taken from the present work and the compilation of [26]) are compared with the $0\hbar\omega$ calculations of Caurier *et al.* [13] in Fig. 2b and Fig. 2c. The data on the $N = 16$ isotopes (^{26}Ne, ^{28}Mg) are well reproduced by the $0\hbar\omega$ calculations, so there is no evidence that $2\hbar\omega$ configurations significantly influence the ground state and 2_1^+ states in these nuclei. The data on the $N = 18$ isotope ^{30}Mg are also well reproduced by the $0\hbar\omega$ calculations.

However, the energy of the 2_1^+ state in the $N = 18$ isotope ^{28}Ne is considerably lower than the $0\hbar\omega$ prediction. Such a lowering in the energy of the 2_1^+ state can be understood schematically by the interaction between the $0\hbar\omega$ configuration which dominates the ground state in ^{28}Ne and the more strongly deformed $2\hbar\omega$ configuration which occurs at a higher energy. The mixing of the two 2^+ states causes the phenomenon of level repulsion, with the 2_1^+ state (still dominated by the $0\hbar\omega$ configuration) being pushed to a lower energy than the unmixed $0\hbar\omega$ state. The $0\hbar\omega$ and $2\hbar\omega$ 0^+ states mix as well. However, the energy shift of the 0^+ states due to mixing will be smaller than that of the 2^+ states if the difference between the unperturbed energies of the 0^+ states is larger than that of the 2^+ states. This is likely since the moment of inertia of the $2\hbar\omega$ configuration is larger than that of the $0\hbar\omega$ configuration. Under these circumstances, the excitation energy of the 2_1^+ state - which is mixed - would be lower than the unperturbed energy of the $0\hbar\omega$ 2^+ state. Obviously, a realistic picture is more complicated due to mixing of a larger number of configurations.

Fig. 2b suggests that the energies of the 2_1^+ states in ^{26}Ne and ^{28,30}Mg are not strongly perturbed by level repulsion, but that a strong perturbation occurs in ^{28}Ne. This may indicate that the $0\hbar\omega$ and $2\hbar\omega$ configurations are particularly close in energy in ^{28}Ne. In contrast, Fig. 2c clearly shows that the value of $B(E2; 0_{gs}^+ \rightarrow 2_1^+)$ reported here for ^{32}Mg indicates that this nucleus is squarely in the island of inversion.

Our Coulomb excitation experiment provides information on the reduced matrix elements such as $B(E2; 0_{gs}^+ \rightarrow 2_1^+)$, but does not provide direct information on whether the charge deformation which drives the $E2$ transition is static or dynamic, whether a static deformation is axially symmetric, or whether an axially symmetric deformation is oblate or prolate. In the case of nuclei in the island of inversion (such as ^{32}Mg), the overbinding provides strong evidence for static deformation.

While the spherical shell model has been used extensively to study the nuclei in the vicinity of the island of inversion, the deformed shell model, or Nilsson model, provides another framework for gaining insights about isotopes in this region. If we assume that the nuclei studied here have static quadrupole deformations with axial symmetry, we can

use the Nilsson model [29] to calculate intrinsic quadrupole moments for oblate and prolate shapes to see whether the data provide a preference for one shape over the other. The Nilsson diagram used for the present calculations (generated with $\kappa = 0.08$ and $\mu = 0$ for $s-d$ shell and $\kappa = 0.0635$ and $\mu = 0.0382$ for $p-f$ shell, where $\kappa = -0.5v_{ls}$ and $\mu = -v_{ll}$ [30]) is shown in Fig. 3. The deformation parameter used in the diagram is δ, which is related to the usual spherical harmonic coefficient β_{20} (or just β_2) by $\beta_2 \approx \delta/0.95$. With this Nilsson diagram, the intrinsic electric quadrupole moments Q_0 have been calculated for the nuclei studied here over a range of deformations by summing over the contributions of the individual protons

$$Q_0 = (16\pi/5)^{1/2}\Sigma_\lambda \langle \lambda | r^2 Y_{20} | \lambda \rangle, \tag{1}$$

where λ are the occupied proton orbitals. The intrinsic quadrupole moments are graphed as a function of δ for ^{26,28}Ne and ^{30,32,34}Mg in Fig. 4. The figures do not include quadrupole moment results for the range of small δ values ($-0.1 < \delta < 0.1$) where residual interaction outside of the standard Nilsson model becomes significant. This figure also illustrates the "experimental" intrinsic electric quadrupole moments extracted from the measured $B(E2; 0^+_{gs} \rightarrow 2^+_1)$ values via the equation [30]

$$Q_0 = [(16\pi/5)B(E2; 0^+_{gs} \rightarrow 2^+_1)]^{1/2}. \tag{2}$$

The bands shown in Fig. 4 as dashed lines correspond to the ranges of experimental uncertainty in the present work. Both positive and negative experimental values are shown in the graphs because our experiment cannot discriminate between prolate and oblate shapes. For all the nuclei in Fig. 4, it is clear that the "experimental" quadrupole moments can be reproduced if the nuclei have substantial prolate deformations ($\delta \geq 0.3$). However, the quadrupole moments for all oblate deformation parameters shown have magnitudes which are much larger than the experimental values. These calculations suggest that if these nuclei have static axially symmetric deformations, they are prolate. The validity of this conclusion is supported by the fact that self-consistent calculations of the mass quadrupole moment in this model agree well with the assumed value of the deformation parameter.

This argument that ^{32}Mg is prolate is consistent with the results of Refs. [5,13] in which the spherical shell model is used. Otsuka [31] raised the possibility that ^{32}Mg is *not* axially symmetric, but is instead γ-unstable. The present calculations cannot exclude this possibility.

In conclusion, we have measured $E(2_1^+)$ and $B(E2; 0_{gs}^+ \rightarrow 2_1^+)$ in ^{26,28}Ne and ^{30,32}Mg. Our measurements of $B(E2; 0_{gs}^+ \rightarrow 2_1^+)$ for ^{26,28}Ne and ^{30}Mg are the first ever reported. In addition, we have placed an upper limit on $B(E2; 0_{gs}^+ \rightarrow 2_1^+)$ in ^{34}Mg. We find that the behavior of ^{26}Ne and ^{30}Mg can be understood in a simple $0\hbar\omega$ framework, but that the $E(2_1^+)$ result for ^{28}Ne suggests that coexisting shapes resulting from competing $0\hbar\omega$ and $2\hbar\omega$ configurations strongly interact in this nucleus. The present and previous results on ^{32}Mg clearly show that $2\hbar\omega$ configurations dominate in this nucleus. Nilsson model calculations presented here suggest that if these nuclei have static axially symmetric deformations, they are prolate.

This work was supported by the National Science Foundation through grants PHY-9523974, PHY-9528844, and PHY-9605207.

REFERENCES

[1] C. Thibault *et al.*, Phys. Rev. C12 (1975) 644.

[2] W. Chung and B.H. Wildenthal, Phys. Rev. C22 (1980) 2260.

[3] C. Dètraz *et al.*, Nucl. Phys. A394 (1983) 378.

[4] D.J. Viera *et al.*, Phys. Rev. Lett. 57 (1986) 3253.

[5] E.K. Warburton, J.A. Becker and B.A. Brown, Phys. Rev. C41 (1990) 1147.

[6] C. Dètraz *et al.*, Phys. Rev. C19 (1979) 164.

[7] T. Motobayashi *et al.*, Phys. Lett. B 346 (1995) 9.

[8] X. Campi *et al.*, Nucl. Phys. A251 (1975) 193.

[9] A. Watt *et al.*, J. Phys. G 7 (1981) L145.

[10] A. Poves and J. Retamosa, Phys. Lett. B 184 (1987) 311.

[11] N. Fukunishi, T. Otsuka and T. Sebe, Phys. Lett. B 296 (1992) 279.

[12] A. Poves and J. Retamosa, Nucl. Phys. A571 (1994) 221.

[13] E. Caurier *al.*, Phys. Rev. C58 (1998) 2033.

[14] Y. Utsuno, T. Otsuka, T. Mizusaki, and M. Honma (to be published).

[15] K. Heyde and J.L. Wood, J. Phys. G 17 (1991) 135.

[16] Z. Ren *et al.*, Phys. Lett. B 380 (1996) 241.

[17] J. Terasaki *et al.*, Nucl. Phys. A621 (1997) 706.

[18] G.A. Lalazissis, A.R. Farhan and M.M. Sharma, Nucl. Phys. A628 (1998) 221.

[19] T. Glasmacher, Annu. Rev. Nucl. Part. Sci. 48 (1998) 1.

[20] B. M. Sherill *et al.*, Nucl. Instr. Meth. B 56 (1991) 1106.

[21] H. Scheit *et al.*, Nucl. Instr. Meth. A 422 (1999) 124.

[22] M.J. Lopez-Jimenez *et al.*, contribution to XXXVII International Winter meeting on Nuclear Physics (Bormio, Italy, January 1999), preprint GANIL P 99 08.

[23] D. Guillemaud-Mueller *et al.*, Nucl. Phys. A426 (1984) 37.

[24] G. Klotz *et al.*, Phys. Rev. C47 (1993) 2502.

[25] A. Winther and K. Alder, Nucl. Phys. A319 (1979) 518.

[26] P.M. Endt, Nucl. Phys. A521 (1990) 1.

[27] P.M. Endt, At. Data Nucl. Data Tables 55 (1993) 171.

[28] G. Audi and A.H. Wapstra, Nucl. Phys. A565 (1993) 1.

[29] S.G. Nilsson and I. Ragnarsson, Shapes and Shells in Nuclear Structure (Cambridge University Press, Cambridge, 1995).

[30] A. Bohr and B.R. Mottelson, Nuclear Structure, Vol.2, (World Scientific, 1998).

[31] T. Otsuka, Nucl. Phys. A616 (1997) 406c.

TABLES

TABLE I. Experimental parameters and results.

	E_{beam} (MeV/A)	Total beam particles/10^6	$E(2_1^+)$ (keV) present	$E(2_1^+)$ (keV) previous	$\sigma(0^+_{g.s.} \rightarrow 2^+)$ (mb)	$B(E2; 0^+_{g.s.} \rightarrow 2^+)$ (e^2fm^4) present	$B(E2; 0^+_{g.s.} \rightarrow 2^+)$ (e^2fm^4) previous
^{26}Ne	41.7	39.83	1990(12)	2010[a]	74(13)	228(41)	
^{28}Ne	53.0	1.46	1320(20)	1320[a]	68(34)	269(136)	
^{30}Mg	36.5	98.35	1481(3)	1482.2(4)[b]	78(7)	295(26)	
^{32}Mg	57.8	6.46	885(9)	885.5(7)[b]	80(17)	333(70)	454(78)[c]
^{34}Mg[d]	50.6	0.22			≤ 164	≤ 670	

[a]Ref. [22]

[b]Ref. [26]

[c]Ref. [7]

[d]See text for explanation of listed results on this nucleus.

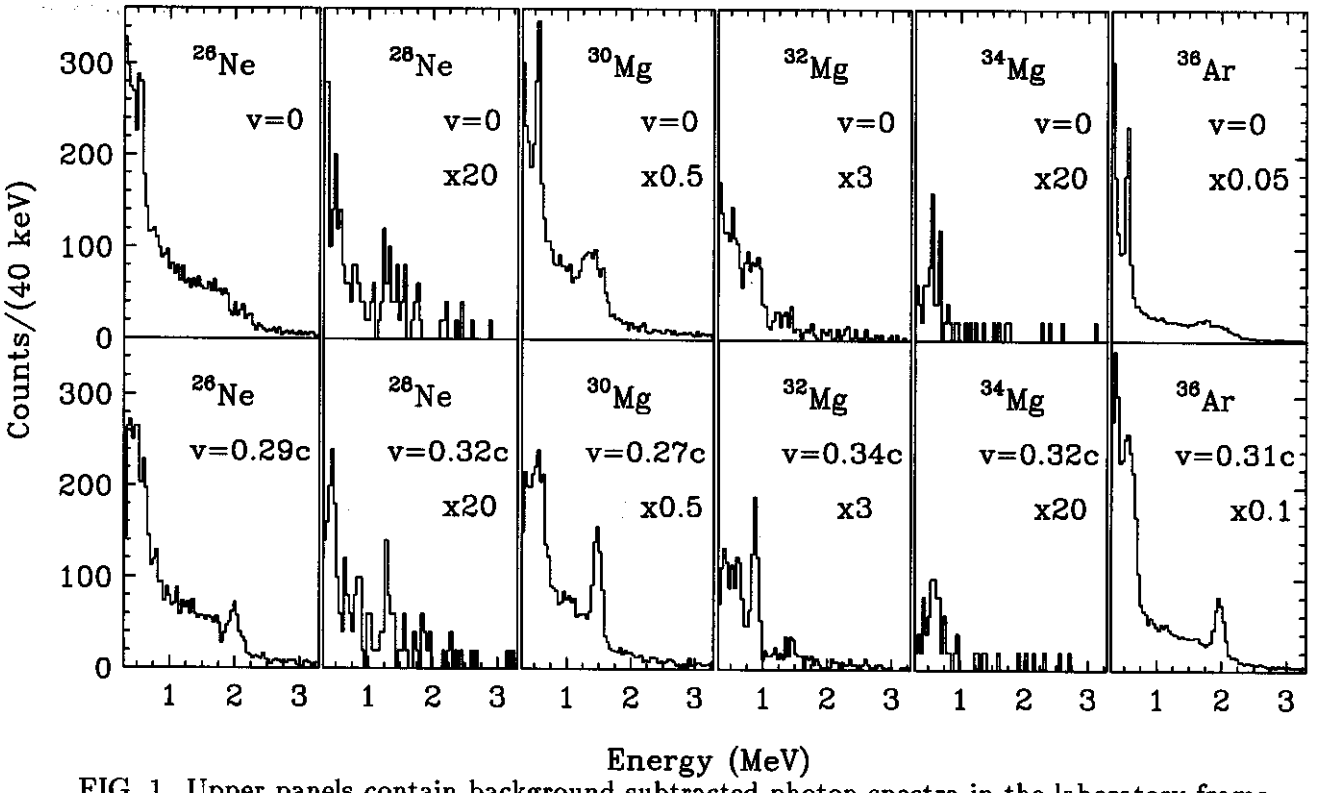

FIG. 1. Upper panels contain background subtracted photon spectra in the laboratory frame. The 547 keV ($7/2^+ \rightarrow g.s.$) transition in the gold target is visible as a peak, while the ($2^+ \rightarrow g.s.$) transitions in each projectile are very broad. Lower panels contain Doppler-corrected, background-subtracted γ-ray spectra.

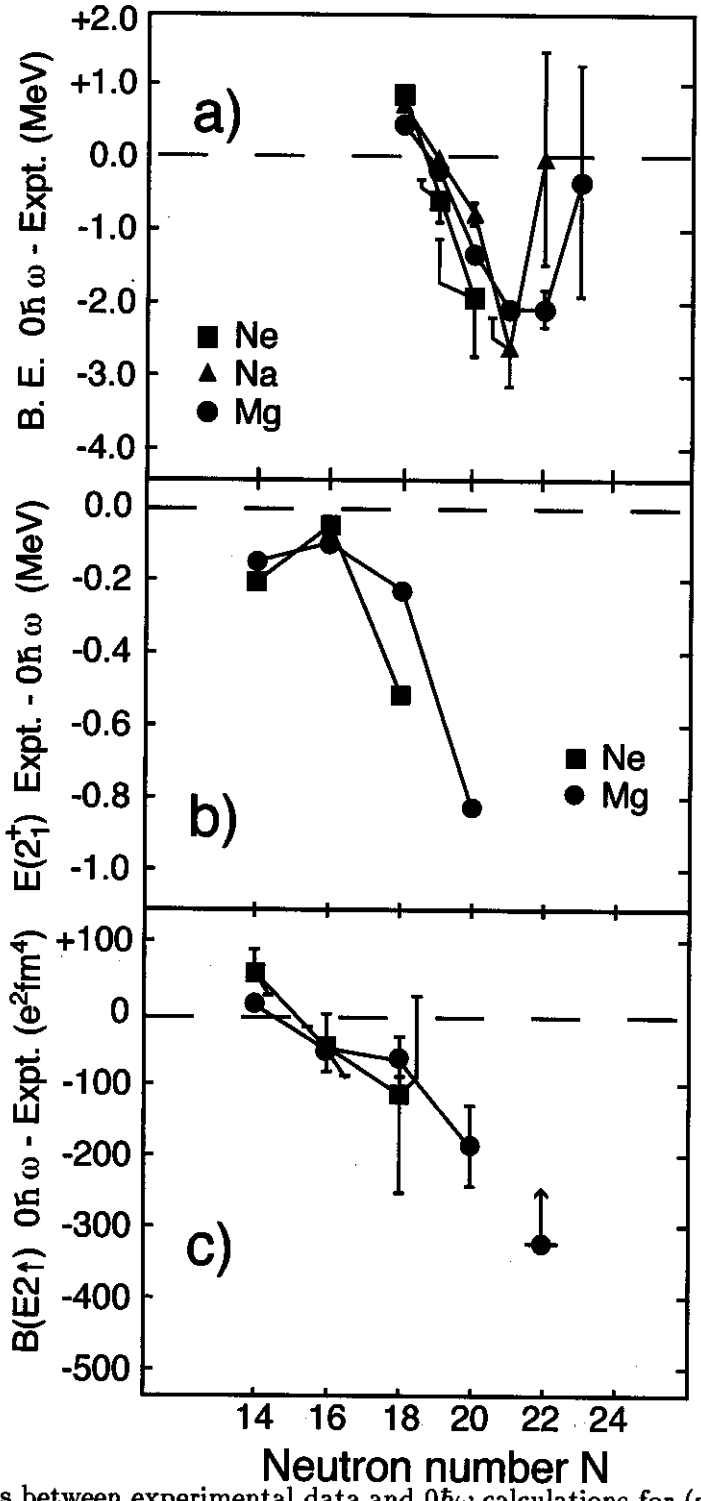

FIG. 2. Differences between experimental data and $0\hbar\omega$ calculations for (a) binding energies in Ne, Na and Mg isotopes; (b) energies of 2_1^+ states in Ne and Mg isotopes; and (c) $B(E2; 0_{gs}^+ \rightarrow 2_1^+)$ values in Ne and Mg isotopes.

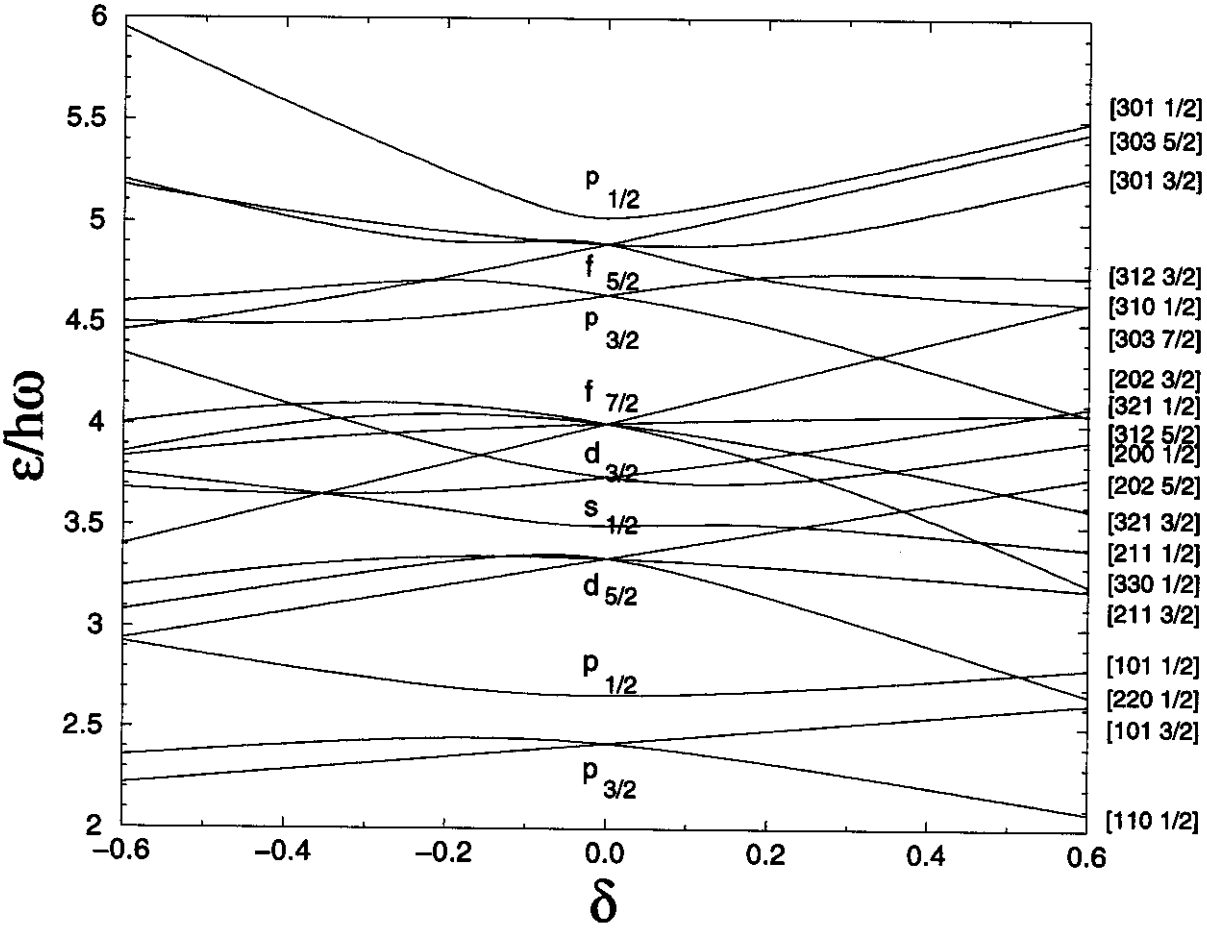

FIG. 3. The Nilsson model diagram used for the calculations described in the text.

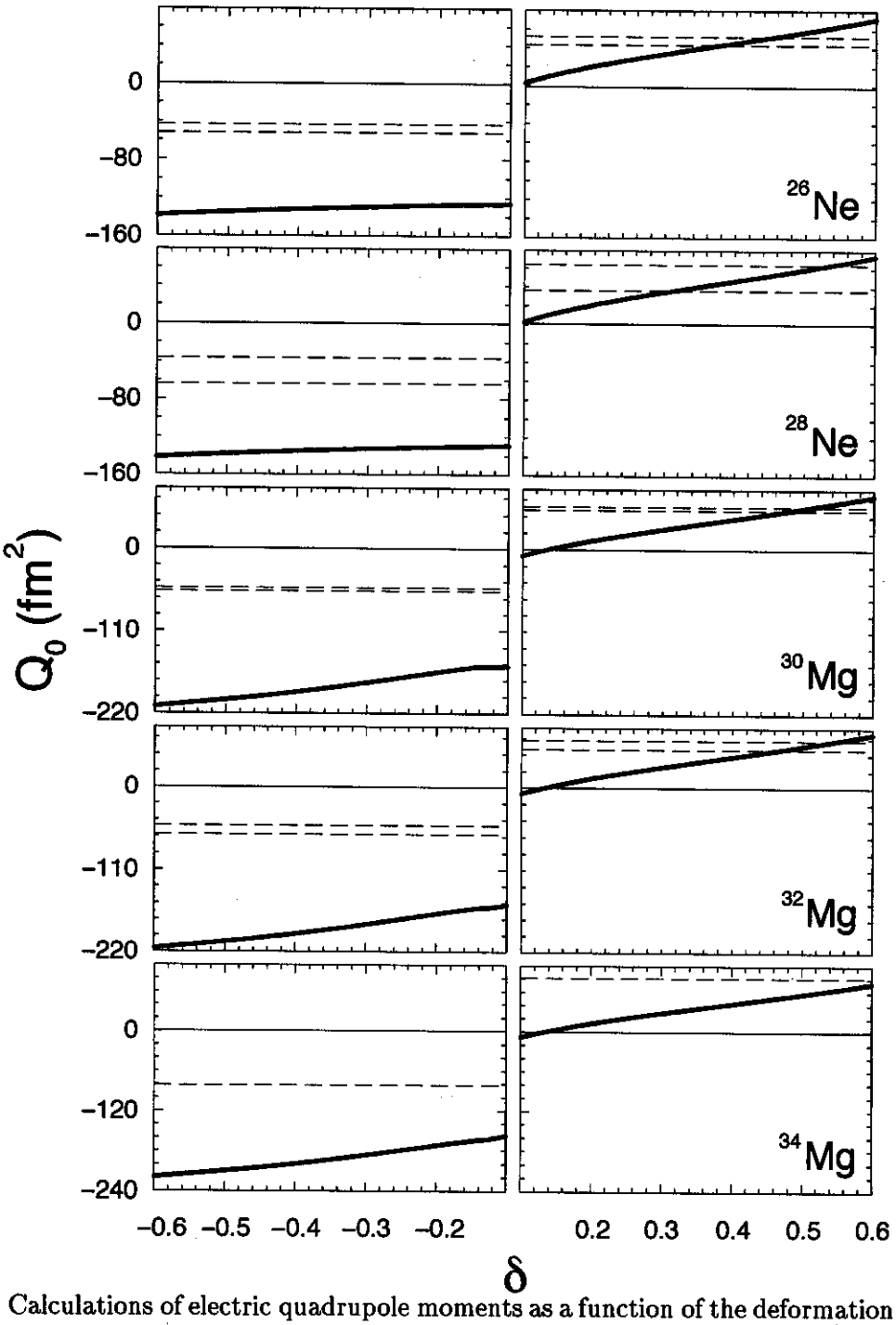

FIG. 4. Calculations of electric quadrupole moments as a function of the deformation parameter δ for ^{26,28}Ne and ^{30,32,34}Mg. The "experimental" electric quadrupole moments in ^{26,28}Ne and ^{30,32}Mg are shown as bands bounded by dashed lines corresponding to experimental uncertainties. The bands are located at both positive and negative values since the present data do not distinguish between prolate and oblate shapes. In ^{34}Mg, the dashed lines correspond to the upper limit on the magnitude of the quadrupole moment.